

# HYDRODYNAMICS OF TWO DEVICES FOR WAVE-POWER EXTRACTION

CHIANG C. MEI\*

*Department of Civil & Environmental Engineering,  
Massachusetts Institute of Technology,  
77 Massachusetts Avenue, Cambridge MA 02139, USA  
\*E-mail: cmei@mit.edu*

We describe the theories for two types of wave-power absorbers that can have a wide bandwidth of high efficiency. One is a compact array of small buoys supported by a large platform. Because each buoy is much smaller than the wavelength, inertia is negligible hence the buoys are not resonated. However the efficiency of the array has a relatively broad frequency band. We shall show that such an array can be more advantageous than a single large buoy of the same total volume. The second device is an oscillating water column attached either to a thin breakwater or to a cliff-like coast. We show that the system has an added inertia that varies with the wavenumber as a N-shaped curve. If the volume of chamber above the interior water surface is suitably chosen, the compressible air serves as a negative spring that broadens the efficiency bandwidth.

## 1. Introduction

For the economy of transmission and storage, wave-power absorbers are best installed not far from the coast. According to the physics of refraction, when ocean waves enter shallow waters, the crests tend to become parallel to the depth contours which are more or less parallel to the shore line. Therefore the wave power potential can be crudely estimated by the power influx per unit length of the coastline. Consider a train of simple monochromatic waves of frequency  $\omega$  and amplitude  $A$ . It is known that the energy per unit length of the wave front is  $E = \frac{1}{2}\rho g A^2$ , and is transported by the group velocity  $C_g$ . The period-averaged rate of power influx per unit length is  $\frac{1}{2}\rho g A^2 C_g$ . If the annual average of the amplitude is  $A = 1$  m then the averaged wave power influx is 40 kW per meter of the coast. Based on statistical data of wave climate, estimates of the wave power potential for many coastal sites in the world are now available.

There are now many designs of single unit absorbers for extracting wave energy. To achieve the capacity of a standard power plant, an array of many units will be needed. Therefore the design challenge is not only in maximizing the efficiency of single units for a broad range of frequencies, but also in optimizing the array configuration so as to make the interference not destructive. To date major efforts appear to have focussed on the development of single units. Each unit can involve

floating bodies or a fixed structures. In the floating body category, there are (i) point absorbers such as a buoy which is insensitive to the direction of incoming waves, (ii) beam-sea devices which are parallel to the front of incoming waves such as Salter's duck, and (iii) head-sea devices which is moored at the bow and can align itself with the direction of incoming waves. Cockerel's raft and its more advanced extension the Pelamis are representative. In the category of fixed structures the oscillating wave column has been much studied. Through a submerged opening the free surface inside the column can oscillate vertically and drive the dry air through a Wells turbine above.

Nearly all of the single-unit absorbers are designed on the basis of impedance matching. The typical mechanical principle is represented by a single buoy connected to a energy absorber which is modeled as a linear damper. In particular, the rate of energy removal is characterized by the product  $kL$  where  $L$  is the capture width and  $k$  the incident wavenumber. In normalized form the capture width  $L$  is

$$kL \equiv \frac{k}{C_g} \frac{\lambda_g \omega^2 |F_z^D|^2}{\omega^2 (\lambda_{zz} + \lambda_g)^2 + (\pi a^2 - \omega^2 (M + \mu_{zz}))^2} \quad (1)$$

where  $F_z^D$  is the heave exciting force on the buoy,  $a$  the buoy radius,  $M$  the buoy mass.  $\mu_{zz}$  and  $\lambda_{zz}$  are respectively the hydrodynamic added mass and radiation damping, and  $\lambda_g$  the absorption coefficient of the power takeoff, all suitably normalized. It can be shown analytically and numerically that

- The maximum energy extraction is achieved at resonance

$$\pi a^2 - \omega^2 (M + \mu_{zz}) = 0 \quad (2)$$

and the extraction rate equals the radiation damping rate

$$\lambda_g = \lambda_{zz}. \quad (3)$$

At best the maximum capture width for a buoy with only one degree of freedom (heave) is such that  $kL = 1$ . To achieve this maximum it is necessary to choose the buoy size so that the resonance frequency coincides with the peak frequency of the incoming sea spectrum. For one system, this maximum is attained only for one frequency.

- The resonance frequency at which this maximum occurs satisfies the order equality  $k_N a = O(1)$ . Thus the buoys radius must be as large as large as  $1/6$  of a wavelength for resonance to occur. A small buoy can only be resonated at a very high frequency.
- The bandwidth of the resonance peak increases as the size of the buoy decreases.

Thus it is difficult for one buoy to be resonated at a low frequency typical of the peak of usual sea spectrum, and to have a wide bandwidth of high efficiency.

To improve the frequency bandwidth of absorption efficiency, phase control of the power-takeoff system has been the most prominent candidate.<sup>1,2</sup> As an alternative,

three groups have recently proposed similar designs that are not based on impedance matching. Each of them involves a compact array of small buoys gathered on a large platform. One is the FO3 system initiated by Fred Olsen in Norway and being developed by ABB & Associates<sup>a</sup>. The second is the Manchester Bobber system initiated by Peter Stansby in UK<sup>b</sup>. In both systems the platform is a square in plan form. The Wave Star<sup>c</sup>, the third system under development in Denmark, has only two rows of small buoys lined along two sides of a long beam. In §2 we shall sketch a recent work by<sup>3</sup> on small buoys in a compact array, relevant to both the FO3 and the Manchester Bobber.

To limit the cost of construction, maintenance, energy storage and transmission, etc., some wave power devices will likely be installed on the coast. In 1985 a test model of OWC was installed on a cliff at Toftestallen, near Bergen, Norway. Since 1990 an OWC pilot plant has been in operation on the coast of Pico, Island of Azores, Portugal.<sup>4</sup> New plans have been under consideration for another full-size OWC station at the head of a breakwater at the mouth of Foz do Douro River, Portugal.<sup>5</sup> The proximity of coastline affects the wave climate near the absorber, hence its performance. In §3 we shall discuss an OWC at the the tip of a breakwater,<sup>7</sup> and in §4 an OWC along a cliff coast.<sup>6</sup>

In thei presentation most of the ideas and results are reviewed. Numerical results and graphs hacan be found in the cited references and will not be repeated here.

## 2. Compact array of small buoys

We consider an array of small buoys supported by a common platform whose horizontal dimension  $L$  is comparable to the incident wavelength  $2\pi/k$  and the sea depth  $h$ . The radius  $a$  of and spacing  $d$  between the buoys are comparable but are much smaller than the sea depth. Owing to the presence of two vastly different length scales (the macroscale ( $L \sim 2\pi/k \sim h$ ) and the micro-scale  $a \sim d$  with  $a/h = \mu \ll 1$ ), a formal theory based on homogenization can be developed.<sup>3</sup> Here we shall give a more physical derivation.

### 2.1. Averaged governing equations

Let us first give a heuristic derivation of the governing equations for the macro-scale motion averaged over the micro-scale. In the fluid, we have

$$\nabla^2 \phi = 0, \quad -h < z < 0, \quad (4)$$

Assume the seabed to be horizontal. then

$$\frac{\partial \phi}{\partial z} = 0, \quad z = -1. \quad (5)$$

---

<sup>a</sup><http://www.abb.com/>

<sup>b</sup><http://www.manchesterbobber.com/>

<sup>c</sup><http://www.WaveStarEnergy.com>

On the mean free surface away from the buoys, the kinematic and dynamic conditions combine to give

$$\frac{\partial \phi}{\partial z} - \frac{\omega^2}{g} \phi = 0, \quad z = 0 \quad (6)$$

On the free surface covered by buoys, let us consider one small buoy first. Assuming that the buoy radius and draft to be small compared to the wavelength, continuity of vertical velocity requires

$$\frac{\partial \phi}{\partial z} = \frac{\partial \zeta}{\partial t}, \quad z = 0 \quad (7)$$

where  $\zeta$  denotes the heave displacement. Modeling the effect of power-takeoff by a linear damping force  $-\lambda_g \frac{\partial \zeta}{\partial t}$  on the buoy where  $\lambda_g$  is the damping coefficient, Newton's law for the buoy requires,

$$M \frac{\partial^2 \zeta}{\partial t^2} = -\pi a^2 \rho \left( g \zeta + \frac{\partial \langle \phi \rangle}{\partial t} \right) - \lambda_g \frac{\partial \zeta}{\partial t}, \quad z = 0 \quad (8)$$

where  $\langle \cdot \rangle$  denotes the spatial average over the bottom of the buoy. For small buoys both conditions can be approximately applied on the mean sea level  $z = 0$ . Since the typical length scale of  $\phi$  is much larger than the size of the buoy,  $\langle \phi \rangle$  can be approximated by  $\phi$  in (8). Eliminating  $\zeta$  we get a condition for  $\phi$  only,

$$\left( M \frac{\partial^2}{\partial t^2} + \rho g \pi a^2 + \lambda_g \frac{\partial}{\partial t} \right) \frac{\partial \phi}{\partial z} + \rho \pi a^2 \frac{\partial^2 \phi}{\partial t^2} = 0. \quad z = 0. \quad (9)$$

For simple harmonic motion (9) becomes

$$\left( 1 - \frac{M \omega^2 + i \lambda_g \omega}{\rho g \pi a^2} \right) \frac{\partial \phi}{\partial z} - \frac{\omega^2}{g} \phi = 0. \quad (10)$$

The above condition is applied at  $z = 0$ . By Archimedes principle  $M = \rho \pi a^2 H$  where  $H$  is the small draft. The ratio  $M \omega^2 / (\rho g \pi a^2) = \omega^2 H / g = O(\mu)$  is small, hence buoy inertia is negligible to the first order of approximation.

From here on we turn to dimensionless quantities defined by

$$\begin{aligned} x &\rightarrow hx, \quad t \rightarrow t\sqrt{hg}, \quad p \rightarrow \rho g A p, \quad \phi \rightarrow \phi A \sqrt{gh}, \quad k \rightarrow \frac{k}{h}, \\ a &\rightarrow ha, \quad \omega \rightarrow \omega \sqrt{gh}, \quad \lambda_g \rightarrow \lambda_g \rho g \pi a^2 \sqrt{\frac{h}{g}}. \end{aligned} \quad (11)$$

Eq. (10) reads, in dimensionless form,

$$\frac{\partial \phi}{\partial z} - \frac{\omega^2}{1 - i \lambda_g \omega} \phi = 0, \quad z = 0, \quad (12)$$

under each buoy. Let  $f$  be the area fraction of the free surface covered by buoys, then the averaged free surface condition is

$$(1 - f) \left( \frac{\partial \phi}{\partial z} - \omega^2 \phi \right) + f \left( \frac{\partial \phi}{\partial z} - \frac{\omega^2}{1 - i \lambda_g \omega} \phi \right) = 0, \quad (13)$$

which leads to one macro-scale condition is obtained for the velocity potential on the buoy-covered surface,

$$\boxed{\frac{\partial \phi}{\partial z} - \omega^2 [1 + f(\mathcal{F}_0 - 1)] \phi = 0, \quad z = 0,} \quad (14)$$

where

$$f \equiv \frac{\pi a^2}{d^2} \quad (15)$$

is the area fraction of solid, or the *packing ratio*,  $d = d^*/h^*$  is the dimensionless spacing and

$$\mathcal{F}_0(\omega) = \frac{1}{1 - i\lambda_g \omega} \quad (16)$$

expresses the effect of the energy absorber. For circular cylinders in a square array,  $a \leq d/2$ , hence  $0 < f < \frac{\pi}{4}$ .

Once the macro-scale variation of the velocity potential is found, the buoy displacement is given by

$$-i\omega \zeta = \frac{\partial \phi}{\partial z} \quad (17)$$

which becomes

$$\zeta = i\omega \mathcal{F}_0(\omega) \phi|_{z=0}. \quad (18)$$

after using (12).

## 2.2. Solving the macroscale problem

Outside the area covered by the buoys, the potential can be expanded as follows

$$\phi = \sum_{n=0}^{\infty} \psi_n(x, y) Z_n(z) \quad (19)$$

where, for  $n = 0$ ,

$$Z_0(z) = \frac{\cosh k(z+1)}{N^{1/2}}, \quad N_0 = \frac{1}{2} \left( 1 + \frac{2k}{\sinh 2k} \right) \quad (20)$$

$$\frac{\partial^2 \psi_0}{\partial x^2} + \frac{\partial^2 \psi_0}{\partial y^2} + k^2 \psi_0 = 0 \quad (21)$$

and  $k$  is the real root of

$$\omega^2 = k \tanh k \quad (22)$$

For  $n = 1, 2, 3, \dots$ ,

$$Z_n(z) = \frac{\cos \kappa_n(z+1)}{N_n^{1/2}}, \quad N_n = \frac{1}{2} \left( 1 + \frac{\sin 2\kappa_n}{2\kappa_n} \right) \quad (23)$$

$$\frac{\partial^2 \psi_n}{\partial x^2} + \frac{\partial^2 \psi_n}{\partial y^2} - \kappa_n^2 \psi_0 = 0, \quad n = 1, 2, 3, \dots \quad (24)$$

where  $\kappa_n$  are the real roots of

$$-\omega^2 = \kappa_n \tan \kappa_n, \quad n = 1, 2, 3, \dots \quad (25)$$

The vertical eigenfunctions  $Z_n(z), n = 0, 1, 2, 3, \dots$  forms an orthonormal set over the range  $-1 < z < 0$ .

Within the buoy-covered area, we also assume a separable solution  $\phi = \Psi(x, y)F(z)$ . It can be shown that the function  $F$  must satisfy the eigen-value problem

$$\begin{aligned} F_{zz}(z) - K^2 F(z) &= 0 & -1 < z < 0 \\ (F_z - \sigma^2 F) &= 0 & z = 0 \\ F_z &= 0, & z = -1, \end{aligned} \quad (26)$$

where

$$\sigma^2 \equiv \omega^2 [f \mathcal{F}_0(\omega) + (1 - f)] \quad (27)$$

and is complex due to energy extraction. There is a discretely infinite set of complex eigenvalues  $K_n$  which are the roots of the complex dispersion relation

$$\sigma^2 = K_n \tanh K_n, \quad n = 0, 1, 2, 3, \dots \quad (28)$$

The corresponding eigenfunctions  $F_n$  are also complex

$$F_n = C_n \cosh K_n(z + 1) \quad (29)$$

where the coefficients  $\{C_n\}$

$$C_n = \sqrt{\frac{2}{\sigma^{-2} \sinh^2(K_n) + 1}} \quad (30)$$

is chosen so that the eigenfunctions  $\{F_n\}$  are orthonormal,

$$\langle F_n | F_m \rangle \equiv \int_{-1}^0 F_n(z) F_m(z) dz = \delta_{nm} \quad (31)$$

For a given frequency  $\omega$ , packing ratio  $f$  and damping rate  $\lambda$ ,  $\sigma$  is first defined.  $K_n$  and  $F_n$  are found numerically. The general solution under the buoys is then,

$$\phi(\mathbf{x}) = \sum_{n=0}^{\infty} \Psi_n(x, y) F_n(z) \quad (32)$$

Now the three-dimensional problem can be reduced to an infinite set of two-dimensional boundary-value problems for  $\psi_n(x, y), \Psi_n(x, y)$ , which depend on the array geometry. We have worked out solutions for two simple arrays.

Strip array: For an infinitely long strip array of total width  $W$  with its edges parallel to the crests of incoming plane waves, we impose the continuity of mass flux and pressure at the edges of the array. The potential in and outside the array can

be solved by using eigenfunction expansions. Let  $R$  and  $T$  denote the reflection and transmission coefficients respectively. Then  $\mathcal{E}$ , the ratio of power absorption rate to the incoming power flux per unit crest length, is found by energy conservation

$$\mathcal{E} = 1 - |T|^2 - |R|^2, \quad (33)$$

which measures the efficiency of power extraction. Computed results show that larger  $W$  leads to a higher efficiency. The gain of  $\mathcal{E}$  by using a wider array is the most important at low frequency. For a given sea spectrum at a specific site, such information can help determine the optimal width of a strip-array based on efficiency and construction costs. In general scattering is significant, hence the maximum efficiency of energy extraction is somewhat lower than that a large beam-sea device such as a Salter's duck. Details can be found in.<sup>3</sup>

Circular array:

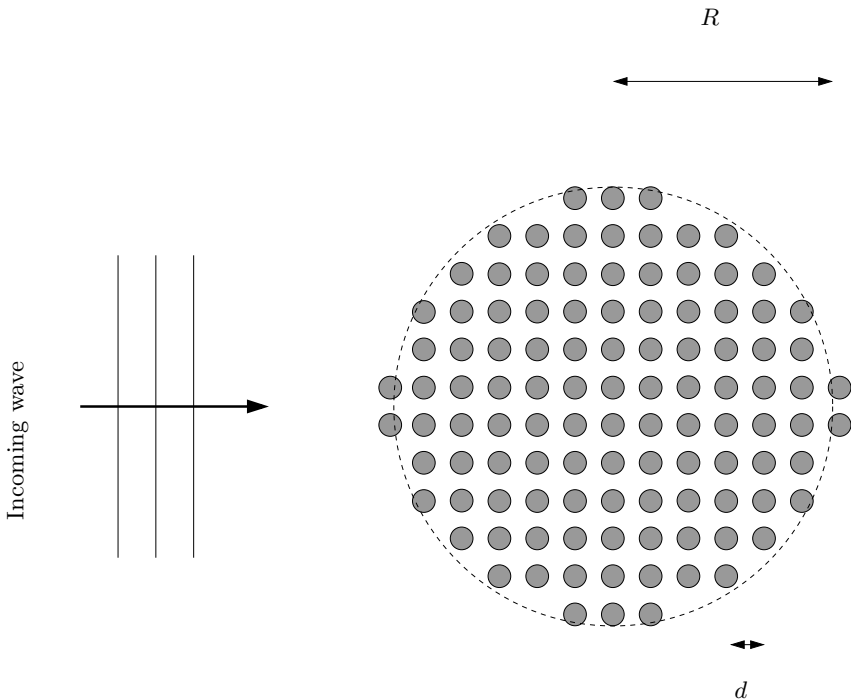


Fig. 1. A circular array of energy-absorbing buoys.

Unlike the square platforms in current designs of FO3 and Manchester Bobber, it is analytically easier to treat an array of buoys supported on a circular platform of radius  $R$ , as shown in Fig. 1. Once the velocity potential is obtained, the absorbed power can be evaluated either from the far field wave amplitude or from the buoy displacement. .

Similar to a large single buoy, a larger circular array yields more energy at low frequency, and there exists an optimal value for the damping rate. We have also examined the ratio

$$\mathcal{E} = L/2R \quad (34)$$

as an alternative measure of efficiency. It is found that a circular array never absorbs more energy than what enters across a diameter of the array. Plots are omitted here.

We have compared the capture widths  $kL$  for three circular arrays with three single buoys. The arrays have the overall dimensionless radii of  $R = (0.5, 1, 2)$ . The draft of each single buoy is assumed to be the same as its dimensionless radius  $a_b$ , and is chosen so as to have the same total volume as all the small buoys in the comparison array of overall radius  $R$ . The draft of a small buoy is  $H$ . In normalized form the volume of a single buoy of radius  $a_b$  and draft  $a_b$  is  $\pi a_b^3$  and the total volume of the buoys in a rig is  $f\pi R^2 H$ . Equating the two we get  $a_b = (fR^2 H)^{1/3}$ . The capture widths for three single buoys with radius  $a_b = 0.17, 0.27, 0.43$  have been computed and compared with three compact arrays with  $R = 0.5, 1$  and  $5$ . For the single buoys the extraction rate is chosen to be the optimum at the peak. It is found that the capture widths of all single arrays are mountain-shaped with the peak value  $kL = 1$ . The peak is increasingly broader for smaller arrays and occur at higher frequencies. All compact arrays have monotonically increasing  $kL$  with the normalized  $k$ , equivalent to the dimensional  $kh$ . Arrays with  $R = 1$  and  $5$  have  $kL$  larger than the single buoy of equal volume. Therefore, the compact arrays are indeed hydrodynamically very promising. The results give theoretical support of the ideas advanced by the FO3 and Manchester Bobber teams.

For future extension it would be interesting to study whether the rate of energy extraction for each buoy can be separately controlled to increase the overall efficiency, and the potential of dozens or hundreds of these platforms in a large array. Mooring systems, nonlinear effects of finite-amplitude waves and frictional loss due to flow separation must all be considered for more comprehensive mathematical modeling of actual designs. These and the questions of cost and safety are worth further study.

### 3. OWC at the tip of a breakwater

Recently<sup>7</sup> have considered an idealized model of an OWC at the tip of a thin breakwater as sketched in sketched in Figures 2. The sea depth is assumed to be constant everywhere. Wells turbines are assumed to be installed on top of the cylindrical column. Special emphasis is on the effect of air compressibility in the pneumatic chamber on the bandwidth of power capture length. This geometry is a special cases of an OWC at the tip of wedge-like coast.

Within the framework of linearization, the total potential in water can be divided into two parts. The first part is due to diffraction of the incident waves by the structure, with the water surface everywhere free of atmospheric pressure. The

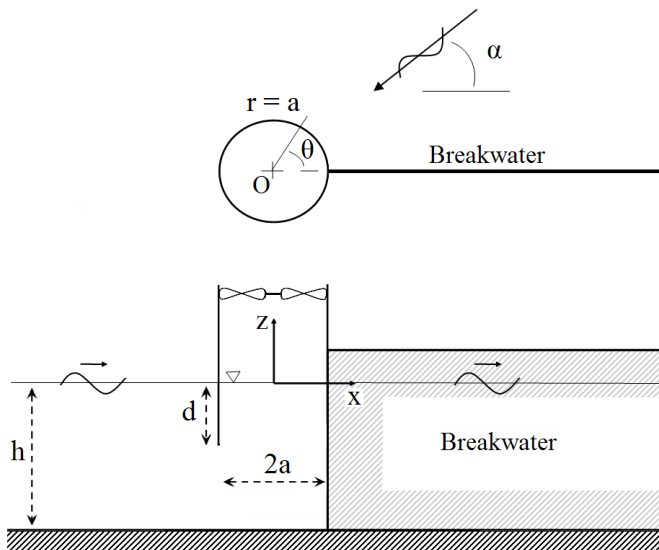


Fig. 2. OWC at the head of a breakwater.

second part is due to the radiation of waves forced by the oscillating air pressure in the chamber above the water surface. Finally the pneumatic chamber air pressure is related to the piston action of the moving free surface and the work done by the turbine. Since the free surface motion is contributed by both diffraction and radiation, the two parts are coupled via the chamber pressure. Both the diffraction and radiation problems are complicated by the presence of the geometry of the structure including the underwater opening and the coastline. We first explain the chamber mechanics then the diffraction and radiation problems.

### 3.1. The pneumatic chamber

The relation between power takeoff and the hydrodynamic parameters were first explained by.<sup>8</sup> We assume the mass flux through the Wells turbines to be proportional to the chamber air pressure. Accounting for air compressibility the mass flux of air is related to the turbine characteristics by:

$$\frac{d(\rho_a V)}{dt} = \rho_a \frac{dV}{dt} + V \frac{d\rho_a}{dt} = \frac{KD}{N} p_a \quad (35)$$

where  $N$  is the rotational speed of turbine blades,  $D$  the outer diameter of turbine rotor,  $\rho_a$  the air density and  $V$  the air chamber volume. The empirical coefficient  $K$  depends on the design, the number and setup of turbines.  $dV/dt$  is the rate of total upward displacement of the water surface inside the column. Assuming isentropy we have  $c_a^2(d\rho_a/dt) = dp_a/dt$  where  $c_a$  is the sound velocity in air. Now

$$\frac{dV}{dt} = Q = Q^R + Q^D \quad (36)$$

where  $Q$  is the total vertical flux forced by the water surface in the column, being the sum of contributions by diffraction and radiation. For simple harmonic motion we denote  $Q = \text{Re}(\widehat{Q}e^{-i\omega t})$ ,  $p_a = \text{Re}(\widehat{p}_a e^{-i\omega t})$ , etc. The two complex amplitudes  $\widehat{Q}^R$  and  $\widehat{Q}^D$  can be found from the solutions of diffraction and radiation problems and expressed as

$$\widehat{Q}^R \equiv -(\mathcal{B} - i\mathcal{C})\widehat{p}_a, \quad \text{and} \quad \widehat{Q}^D \equiv \Gamma A_0 \quad (37)$$

where  $\mathcal{B}$  and  $\mathcal{C}$  are real,  $\Gamma$  is complex and  $A_0$  is the incident wave amplitude. Physically  $\mathcal{C}$  amounts to the added hydrodynamic inertia (i.e., the radiation susceptance) and  $\mathcal{B}$  amounts to radiation damping (i.e., radiation conductance). It then follows from (35) that

$$\frac{\widehat{p}_a}{A_0} = \frac{\Gamma}{\left[ \left( \frac{KD}{N\rho_a^0} + \mathcal{B} \right) - i \left( \mathcal{C} + \frac{\omega V_o}{c_a^2 \rho_a^0} \right) \right]} \quad (38)$$

.<sup>8</sup> With this the time-averaged power output can be calculated

$$P_{out} = \frac{d(\rho_a V) p_a}{dt \rho_a^0} = \frac{KD}{2N\rho_a^0} |\widehat{p}_a|^2 \quad (39)$$

In terms of the dimensionless coefficients ,

$$\Gamma = \widetilde{\Gamma} \left( \frac{ag}{\omega} \right), \quad (\mathcal{B}, \mathcal{C}) = (\widetilde{\mathcal{B}}, \widetilde{\mathcal{C}}) \left( \frac{a}{\omega \rho_w} \right), \quad \chi = \frac{\rho_w KD \omega}{\rho_a N a}, \quad \beta = \frac{\omega^2 V_o \rho_w}{c_a^2 a \rho_a} \quad (40)$$

the efficiency of power extraction can be measured by the capture length  $L$  defined by

$$kL = \frac{2kP_{out}}{\rho g A_0^2 C_g} = \frac{gka}{\omega C_g} \frac{\chi |\widetilde{\Gamma}|^2}{(\chi + \widetilde{\mathcal{B}})^2 + (\widetilde{\mathcal{C}} + \beta)^2} \quad (41)$$

Here the parameter  $\chi$  characterizes the turbines,  $\beta$  represents the effect of compressibility of chamber air and is analogous to a spring of negative elasticity.

To obtain the parameters  $\widetilde{\mathcal{B}}$ ,  $\widetilde{\mathcal{C}}$  and  $\widetilde{\Gamma}$ , it is necessary to solve the radiation and diffraction problems.

### 3.2. Diffraction problem

Let the incident wave arrive from the direction  $\theta = \alpha$  with respect the breakwater (see Figure 2). The total diffraction potential outside the cylinder can be expressed as the sum of two parts:

$$\varphi_O(r, \theta, z) = \varphi_1 + \varphi_2 \quad (42)$$

where  $\varphi_1$  is due to scattering by a solid cylinder extending the entire sea depth and connected to the wedge-like coastline, and  $\varphi_2$  is the correction for the opening.

It is fortunate that the first part can be solved exactly as in the following subsection by extending the solution of a vertical wedge by.<sup>9</sup> the result is, in dimensional terms,

$$\varphi_1 = -\frac{igA}{\omega} \frac{Z_0(z)}{Z_0(0)} \eta(r, \theta) \quad (43)$$

where

$$\eta = \sum_{n=0}^{\infty} \frac{\epsilon_n}{\nu\pi} \frac{2\pi i \cos \frac{n\alpha}{\nu} e^{-\frac{in\pi}{2\nu}} Y'_{n/\nu}(ka)}{H'_{n/\nu}(ka)} \left( J_{n/\nu}(kr) - \frac{J'_{n/\nu}(ka)}{Y'_{n/\nu}(ka)} Y_{n/\nu}(kr) \right) \cos \frac{n\theta}{\nu} \quad (44)$$

$$Z_0(z) = \frac{\cosh k(z+h)}{N^{1/2}}, \quad N_0 = \frac{1}{2} \left( 1 + \frac{2kh}{\sinh 2kh} \right) \quad (45)$$

and  $\epsilon_0 = 1$ ;  $\epsilon_n = 2, n = 1, 2, 3, \dots$  are the Jacobi symbols. As a limiting case  $\nu = 2$  gives the diffraction potential for a circular cylinder at the tip of a thin breakwater,

$$\varphi_1 = \frac{-igA_0}{\omega} \sum_{n=0}^{\infty} \epsilon_n \frac{\cos \frac{n\alpha}{2} e^{-\frac{in\pi}{4}} iY'_{n/2}(ka)}{H'_{n/2}(ka)} \left[ J_{n/2}(kr) - \frac{J'_{n/2}(ka)}{Y'_{n/2}(ka)} Y_{n/2}(kr) \right] \cos \left( \frac{n\theta}{2} \right) \frac{Z_0(z)}{Z_0(0)} \quad (46)$$

As another limiting case to be used later,  $\nu = 1$  corresponds to a half cylinder on a straight coast. The potential  $\varphi_I$  can also be found explicitly by the method of images, i.e. by adding the solutions for scattering by a solid cylinder in the open sea to two symmetrically incident plane waves arriving with the angles  $\pi + \alpha$  and  $\pi - \alpha$ ,

$$\varphi_I = \frac{-igA_0}{\omega} \sum_{n=0}^{\infty} \epsilon_n (-i)^n \left( J_n(kr) - \frac{J'_n(ka)}{H'_n(ka)} H_n(kr) \right) \frac{Z_0(z)}{Z_0(0)} \cdot \{ \cos(n[\alpha + \theta]) + \cos(n[\alpha - \theta]) \} \quad (47)$$

The second part  $\varphi_2$  is the correction to  $\varphi_1$  for the opening at  $r = a, 0 < \theta < 2\pi, -h < z < -d$ . The correction potential outside the column must involve both propagating and evanescent modes. The latter correspond to the vertical eigenfunctions in dimensional form

$$Z_\ell(z) = \frac{\cos \kappa_\ell(z+h)}{N_\ell^{1/2}}, \quad N_\ell = \frac{1}{2} \left( 1 + \frac{\sin 2\kappa_\ell h}{2\kappa_\ell h} \right) \quad (48)$$

where  $\kappa_\ell$  are the real roots of

$$-\omega^2 = g\kappa_\ell \tan \kappa_\ell h, \quad \ell = 1, 2, 3, \dots \quad (49)$$

The formal solution is the following expansion

$$\varphi_2 = \frac{-igA_0}{\omega} \sum_{\ell=0}^{\infty} Z_\ell(z) \sum_{n=0}^{\infty} A_{n\ell} \frac{K_{\frac{n}{2}}(\kappa_\ell r)}{\kappa_\ell a K'_{\frac{n}{2}}(\kappa_\ell a)} \cos \frac{n\theta}{2} \quad (50)$$

which satisfies the no-flux condition on both sides the breakwater ( $\theta = 0, 2\pi$ ). In the series the first term with  $\ell = 0$  corresponds to an outgoing wave

$$K_{\frac{n}{2}}(-ikr) = \frac{\pi}{2} i^{\frac{n}{2}+1} H_{\frac{n}{2}}^{(1)}(kr) \tag{51}$$

Inside the cylinder  $r < a, 0 < \theta < 2\pi$ ,  $\varphi_2$  is due entirely to the opening,

$$\varphi_C = \frac{-igA_0}{\omega} \sum_{n=0}^{\infty} \sum_{\ell=0}^{\infty} (B_{n\ell} \cos n\theta + C_{n\ell} \sin n\theta) \frac{I_n(\kappa_{\ell}r)}{\kappa_{\ell}a I'_n(\kappa_{\ell}a)} Z_{\ell}(z) \tag{52}$$

where  $B_{n\ell}$  and  $C_{n\ell}$  are also unknown. Corresponding to  $\ell = 0, \kappa_0 = -ik$  the first term in the series above is to be interpreted as

$$I_{\frac{n}{2}}(-ikr) = (-i)^{\frac{n}{2}} J_{\frac{n}{2}}(kr) \tag{53}$$

Since the radial flux must be continuous at the opening, we require

$$\frac{\partial \varphi_2}{\partial r} = \frac{\partial \varphi_C}{\partial r} = \begin{cases} 0 & -d < z < 0, \\ U(z, \theta) & -h < z < -d, \end{cases} \quad 0 < \theta < 2\pi, \tag{54}$$

Using the expansions for  $\varphi_O = \varphi_1 + \varphi_2$  and  $\varphi_C$ , and invoking orthogonality, we get for any integer  $\ell$  and  $n$ :

$$\frac{2\pi}{\epsilon_n} A_{n,\ell} = \frac{ia\omega}{ghA_0} \int_0^{2\pi} \int_{-h}^{-d} U(\theta, z) Z_{\ell}(z) \cos \frac{n\theta}{2} d\theta dz \tag{55}$$

$$\frac{2\pi}{\epsilon_n} \{B_{n,\ell} ; C_{n,\ell}\} = \frac{ia\omega}{ghA_0} \int_0^{2\pi} \int_{-h}^{-d} U(\theta, z) Z_{\ell}(z) \{\cos(n\theta) ; \sin(n\theta)\} d\theta dz \tag{56}$$

Since the pressure must also be continuous at the opening, we require

$$\varphi_1 + \varphi_2 = \varphi_C, \quad r = a, -h < z < -d \tag{57}$$

we get from (57),

$$\begin{aligned} & \sum_{n=0}^{\infty} \left[ \mathcal{E}_n \cos \frac{n\theta}{2} Z_0(z) + \sum_{\ell=0}^{\infty} A_{n\ell} \frac{K_{\frac{n}{2}}(\kappa_{\ell}a)}{\kappa_{\ell}a K'_{\frac{n}{2}}(\kappa_{\ell}a)} \cos \frac{n\theta}{2} Z_{\ell}(z) \right] \\ & = \sum_{n=0}^{\infty} \sum_{\ell=0}^{\infty} (B_{n\ell} \cos n\theta + C_{n\ell} \sin n\theta) \frac{I_n(\kappa_{\ell}a)}{\kappa_{\ell}a I'_n(\kappa_{\ell}a)} Z_{\ell}(z) \end{aligned} \tag{58}$$

where for brevity:

$$\mathcal{E}_n = \epsilon_n \frac{\cos \frac{n\alpha}{2} e^{-\frac{in\pi}{4}} i Y'_{n/2}(ka)}{Z_0(0) H'_{n/2}(ka)} \left( J_{n/2}(ka) - \frac{J'_{n/2}(ka)}{Y'_{n/2}(ka)} Y_{n/2}(ka) \right) \tag{59}$$

After using (55) and (56), an integral equation for  $U(\theta, z)$  is obtained,

$$\begin{aligned} & \int_0^{2\pi} \int_{-h}^{-d} d\theta' dz' U(z', \theta') \mathcal{K}(z, \theta; z', \theta') = \frac{-2\pi igA_0}{a\omega} \sum_{n=0}^{\infty} \mathcal{E}_n \cos \frac{n\theta}{2} Z_0(z), \\ & 0 < \theta < 2\pi, \quad -h < z < -d \end{aligned} \tag{60}$$

with the kernel:

$$\begin{aligned} \mathcal{K}(z, \theta; z', \theta') \equiv & \\ & \sum_{n=0}^{\infty} \sum_{\ell=0}^{\infty} \frac{\epsilon_n}{h} \frac{I_n(\kappa_{\ell} a)}{\kappa_{\ell} a I'_n(\kappa_{\ell} a)} Z_{\ell}(z) Z_{\ell}(z') [\sin(n\theta) \sin(n\theta') + \cos(n\theta) \cos(n\theta')] \\ & - \sum_{n=0}^{\infty} \sum_{\ell=0}^{\infty} \frac{\epsilon_n}{h} \frac{K_{\frac{n}{2}}(\kappa_{\ell} a)}{\kappa_{\ell} a K'_{\frac{n}{2}}(\kappa_{\ell} a)} Z_{\ell}(z) Z_{\ell}(z') \cos\left(\frac{n\theta}{2}\right) \cos\left(\frac{n\theta'}{2}\right) \end{aligned} \quad (61)$$

This integral equation is solved by an efficient method due to<sup>10</sup> for a similar problem in two dimensions, where  $U(\theta, z)$  is expanded as a Fourier series in  $\theta$  and Chebychev polynomials in  $z$ . The expansion coefficients are found numerically after truncation. Afterwards all the coefficients  $A_{n\ell}$ ,  $B_{n\ell}$  and  $C_{n\ell}$  can be computed from (55) and (56). Then the diffraction potential in the entire fluid is solved

We have computed the free surface elevation inside and around the cylinder for different incidence angles  $\alpha = 0, \pi/4, \pi/2, 3\pi/4$  and  $\pi$  radians, each at resonance of the  $0^{th}$  mode, for  $a/h = 0.5$   $d/h = 0.2$ ,  $ka = 1.27$  and  $t = 0$ . Strond differences are present for the wave paterns outside the coloumn, but the surface inside is relative uniform with little difference. The results can be used to compute the forces on the cylinder.

### 3.3. Radiation Problem

Due to the high sound speed in air and the low frequency of sea waves, the air pressure  $p_a$  is approximately uniform throughout the chamber. The assumption that the breakwater has zero thickness makes the radiation problem axially symmetric. and has been solved by<sup>10</sup> for a circular OWC in the open sea.

For evaluating the energy extracted, the coefficients  $\tilde{\mathcal{B}}$  and  $\tilde{\mathcal{C}}$  have been calculated from (37). For small columns ( $a/h = 0.25, 0.5$ ), the damping is positive in the computed range of  $kh$ . It is found that, unlike the case of a rigid floating body, the added mass  $\tilde{\mathcal{C}}$  changes sign, and is shaped like the letter  $N$ . For  $a/h = 0.25, 0.5$  there is only one  $N$ ; for  $a/h = 1$  there are two, separated by the zero of  $J'(ka)$ . Both the frequency and the amplitude of the resonance peak decrease with increasing  $a/h$ . On the other hand, a larger radius  $a$  leads to a wider bandwidth. Physically, as  $a/h$  becomes smaller, the fluid inside the OWC moves like a solid piston. In the limit a hydrostatic approximation predicts resonance at  $kd \tanh(kh) = 1$  (which corresponds to  $kh \approx 5$ ).

### 3.4. Extracted Power

To achieve maximum efficiency for a single frequency, one can optimize both the turbine characteristics  $\chi$  and the chamber size to get the well-known criteria that  $-\beta(\omega) = \tilde{\mathcal{C}}(\omega)$  and  $\chi(\omega) = \tilde{\mathcal{B}}(\omega)$ . The maximum capture length is:  $kL_{max} = 1$ . It is desirable to strive for high efficiency for a broad band of frequencies. In practice,

it is likely feasible to vary the power-takeoff characteristics such as the number of turbines, blade angle, rotation speed, etc., for a broad range of frequencies, but hardly the dimensions of the column and pneumatic chamber. We shall therefore seek to optimize  $\chi$  over a wide interval of  $kh$  under the constraint of fixed chamber volume  $V_o$ .

By taking  $\partial kL/\partial\chi = 0$ , we get the optimum  $\chi$ :

$$\chi(\omega) = \sqrt{\widetilde{\mathcal{B}}(\omega)^2 + (\widetilde{\mathcal{C}}(\omega) - \beta(\omega))^2} \tag{62}$$

We now assume that the power-takeoff can be controlled so that this condition is satisfied for all  $\omega$  or  $kh$ .

Recall that for maximum capture length,  $-\beta = \widetilde{\mathcal{C}}$ , i.e., the curves  $-\beta$  vs  $kh$  and  $\widetilde{\mathcal{C}}$  vs.  $kh$  must intersect. Numerically the curve of  $\widetilde{\mathcal{C}}$  is found to shape as the letter *N* for  $a/h = 0.25, 0.5$ . Hence there can be two points of intersection, implying two peaks of  $kL$ . For  $a/h = 1$ , the  $\widetilde{\mathcal{C}}$  curve consists of two *N*'s. Hence there are four peaks of  $kL$ . Since  $\beta \propto \omega^2 \propto kh \tanh(kh)$ , the  $\beta$  curve is almost linear in  $kh$  for sufficiently short waves.

In figure 3 we shown the capture width for one non-zero  $\beta$  which can be chosen by varying the chamber volume  $V_o$ . If  $V_o = 0$ , or equivalently, air compressibility is ignored, the  $\beta$  vs  $kh$  curve intersects with the  $\widetilde{\mathcal{C}}$  curve only once, resulting in just one maximum efficiency. As  $V_o$  increases, the  $\beta$  curve is inclined downward, causing two intersection points, hence two maxima and wider bandwidth in efficiency. Further increase of  $V_o$  brings the two intersecting points together. If  $V_o$  exceeds a certain limit, there is no interaction and optimum efficiency cannot be achieved. For any  $a, d$  and  $h$  there is only a finite range of  $V_o$  where  $kL$  is optimum for two different frequencies. Therefore compressibility of air in the finite chamber enables the broadening the bandwidth of the extraction efficiency.

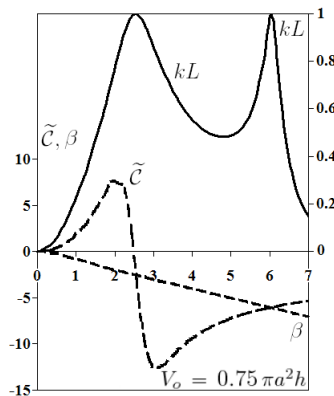


Fig. 3. Capture length (solid), added mass (dashed) and  $\beta$  coefficient (dotted) against the normalized frequency  $kh$  (optimized efficiency) for one pneumatic chamber volume  $V_o = 0.75\pi a^2 h$   $V_o$  and for  $a/h = 0.5, d/h = 0.2, h = 10m$

In<sup>7</sup> it is shown and explained that for this idealized geometry where the breakwater has zero thickness, the averaged water surface elevation inside the column and power extraction is independent of the incidence angle. Thus the thin breakwater has not effect on energy extraction. The efficiency is therefore the same as that of an OWC in the open sea. This feature no longer holds in practice where the width of the breakwater is comparable to the column radius.

#### 4. OWC on a cliff coast

For a vertical OWC on a straight and cliff-like coast, as sketched in Figure 4, the seaside half is open from the seabed to the depth  $z = -d$ . The analyses of the diffraction and radiation problems are similar to that in the last section.<sup>6</sup>

We can examine the power extraction by combining the solutions of the radiation and scattering problems with the power take-off model discussed before. As reasoned before in the last section, it is likely possible to design a controllable power-takeoff system so that  $\chi$  can be varied over a wide frequency range of the incident sea, by changing turbine numbers and speeds, and/or the blade geometry. However, once chosen for one frequency the added mass and radiation damping coefficients  $\tilde{B}(\omega), \tilde{C}(\omega)$  are then fixed for all other frequencies. Again thanks to the  $N$ -shaped curve of the added mass and air compressibility, one can get a broad bandwidth of the absorption efficiency.

By controlling the turbine according to (62) for normal wave incidence only and for a system with the following dimensions:  $h = 10m$ ,  $a/h = 0.5$ ,  $d/h = 0.2$ , and  $V_0 = 2\pi a^2 h$  above water. The corresponding curve of  $\beta = -\omega^2 V_0 \rho_w / c_a^2 a \rho_a$  intersects the added mass curve at four values of  $kh$  (1.8, 3.1, 4.1, 4.5). Hence the  $\chi$ -optimized capture length attains its optimum at these four frequencies and the overall bandwidth is quite broad. By choosing different heights of the column above water, the slope of  $\beta$  can be changed, resulting in a different efficiency curve. It is found that the optimum capture length averaged over all incidence angles is twice the optimum capture length of an offshore device. This is clearly the consequence of coastal reflection which doubles the amplitude of the incident wave.

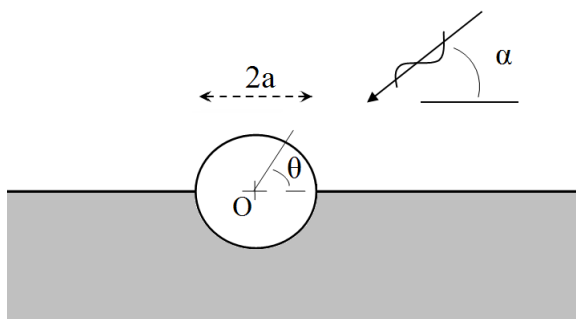


Fig. 4. OWC on a cliff coast.

We have also examined the effects of angle of incidence. Understandably more power is extracted from normally incident waves.

The present theory can be readily modified for a OWC at the corner of wedge-like coast. To take advantage of air compressibility for broadening the frequency range of high efficiency, it appears necessary that the column radius must be fairly large. it remains a design challenge to control the power-takeoff system for a wide range of frequencies.

## 5. Acknowledgements

This article is based on thesis works by X. Garnaud and H. Martins-rivas with the financial support by the Sustainable Energy Program of MIT-Portugal Alliance Project, and from MASDAR Institute of Science and Technology in the program of MIT-Abu Dhabi Alliance. Partial support has also been received from US-Israel Bi-National Science Foundation and from an ignition grant by MIT Earth System Initiative.

## References

1. J. Falnes, *Ocean Waves and Oscillating Systems*. Cambridge University Press (2002).
2. A.F. de Q. Falcao *Ocean Engineering*, **35(3-4)**, 358-366. (2008).
3. X. Garnaud and C.C Mei *J. Fluid Mech.* (2009).
4. A. F. de O. Falcao *Fourth European Wave and Tidal Energy Conf.* Aalborg, Denmark. (2000).
5. Martins et. al . *Sixth European Wave and Tidal Energy Conf.* Glasgow. UK (2005).
6. H. Martins-rivas and C.C. Mei, *J. Fluid Mech.* **626**, 396-414 (2009).
7. H. Martins-rivas and C.C. Mei, *Ocean Engineering*
8. A.Sarmiento and A. F. de O. Falcao *J. Fluid Mech.* **150**, 467-485 (1985).
9. J. J. Stoker *Water Waves*. Wiley. (1958).
10. D. V. Evans and R. Porter, *J. Offshore Mech. Arc.Eng.* **119**, 210 21. (1997).